2

Ultra-Wideband (UWB) Communications Channel – Theory and Measurements

Javad Ahmadi-Shokouh[1] and Robert Caiming Qiu[2]
[1]*University of Sistan and Baluchestan*
[2]*Tennessee Tech University*
Iran
USA

1. Introduction

The most recent increase in demand within the wireless user community for short-range, very high rate data and video transmission devices has motivated the growth of a new generation of broadband wireless access communication systems, i.e. Ultra-Wideband (UWB) radio (1)-(4). UWB technology has been employed for several decades in military and commercial communications applications like high-speed mobile Local Area Networks (LAN), imaging and surveillance systems, ground penetration radars, automotive sensors, medical monitors and recently Wireless Personal Area Networks (WPAN) (5). Spread-spectrum communication systems using ultra-short impulses have seen a renewed interest because of its fine resolution in delay to the order of a tenth of nanosecond though at the cost of a ultra wide frequency band. Low transmission power and large bandwidth together render the power spectral density of the transmitted signal extremely low, which allows the frequency-underlay of a UWB system with other existing radio systems. Hence, the short range radio UWB will play a critical role in the local/home (*pico-cell*) level of the broadband networks due to its unprecedented, broad bandwidth. Indoor wireless systems operate in the areas where usually there is no Line-of-Sight (LOS) radio path between the terminals, the transmitter, and the receiver, and where due to obstructions (furniture, partitions, walls, etc.), multi-diffraction, multi-reflections, and multi-scattering effects occur. These lead to not only additional losses (with regarding those obtained in LOS), but also multipath fading of the signal strength observed at the receiver. Basically, one of the most important aspects of any radio channel-modeling activity is the investigation of the distribution functions of channel parameters. Typically, these distributions are obtained from measurements or simulations based on almost exact or simplified descriptions of the environment. However, such methods often only yield insights into the statistical behavior of the channel and are not able to give a physical explanation of observed channel characteristics. Due to the extremely broad bandwidth, the channel is highly dispersive, even for an individual path. Physics-based models (2) are usually required to understand the multipath pulses waveforms that are necessary for optimal reception.

There exist very good fundamental investigations on the UWB propagation channel characterization and modeling in the literature (6)-(11). More particularly, the references (9) and (11) give an excellent overview of the UWB channels and the authors in (10)

present a very comprehensive tutorial on the UWB channel modeling. To understand the fundamental limits and potential applications of UWB technology, in this paper we will investigate the empirical measurements on the UWB propagations channels. Our focus in this integrated survey lies on the indoor environments, including office, laboratory, commercial and residential buildings. Moreover, we consider some special applications of the UWB systems which have an indoor-like areas, e.g. inside a Magnetic Resonance Imaging (MRI) system, underground mine and so on. A large number of references, more than 100 and mostly recently published, are used in this investigation. The basic channel characterization parameters are extracted and discussed. We review all the channel characterization procedures in this regard. To characterize a UWB propagation indoor channel, a common method is applying a Radio-Frequency (RF) signal to the channel and making an empirical evaluation of the received signal. Through this type of channel characterization, essential metrics are drawn which are: *Path-Loss (PL)*, *large-scale fading*, *small-scale fading*, *multipath arrival rate*, *Power-Delay-Profile (PDP)*, *Root-Mean-Squared (RMS) delay spread*, *temporal correlation*, *Angle-of-Arrival (AOA)*, *spatial correlation across the receiver's spatial aperture*, *Frequency-Selectivity (FSE)* and *Pulse-Distortion (PD)*.
The rest of this paper organized as follows: in Section II, a general formulation of the UWB Channel Impulse Response (CIR) is presented. Section III provides the employed channel characterization procedures and measurement settings. In section IV, we review the channel fading's power-Loss characteristics. A survey on the channel fading's temporal characterizations is presented in Section V. In section VI, the channel fading's spatial characteristics is being reviewed. We then investigate on the channel fading's frequency-dependent characteristics in Section VII. Finally, Section VIII concludes the paper.

2. Multipath Channel Impulse Response (CIR) and basic definitions

A common and convenient model for characterization of the multiptah channel is the discrete-time impulse response model. In this model, the multipath delay axis τ is discretized into equal time delay segments called *bins* (12), (13). Each bin has a time delay width equal to $\Delta\tau = \tau_{i+1} - \tau_i$. Any number of multipath signals received within the ith bin are represented by a single resolvable *multipath component* having delay τ_i (13). A reasonable bin size is the specific measurement's *time resolution* since two paths arriving within a bin cannot be resolved as distinct path. The relative delay of the ith multipath component as compared to the first arriving component is called *excess delay* and if the total number of possible multipath components is N, the *maximum excess delay* of the propagation channel is given by $N\Delta\tau$ (13).
In a multipath propagation channel, since the received signal consists of a series of attenuated, time delay, phase shifted replicas of the transmitted signal, the impulse response of multipath channel can be expressed as (1) (13).

$$h(\tau,t) = \sum_{i=0}^{N(t)-1} a_i(\tau,t)\, e^{j\varphi_i(\tau,t)} \delta(\tau - \tau_i(t)) \tag{1}$$

where $a_i(\tau,t)$, $\varphi_i(\tau,t)$ and $\tau_i(t)$ are the real amplitude, the phase shift and excess delay, respectively, of ith multipath component at time t. Generally, the parameters a_i, φ_i and τ_i are random time-variant functions because of the motion of people and equipment in and around of buildings. However, since the rate of their variations is very slow as compared with the measurement time interval, these parameters can be treated as time-invariant

random variables within one snapshot (bin) of measurement. Moreover these parameters are frequency-dependent since they are related to radio signal characteristics such as transmission and reflections.
The time-invariant CIR (2), assuming a stationary environment, was first suggested in (14) to describe multipath-fading channels. This model has been used successfully in mobile radio applications (12) and can be applied to the UWB indoor propagation channels.

$$h(\tau) = \sum_{i=0}^{N-1} a_i(\tau) e^{j\varphi_i(\tau)} \delta(\tau - \tau_i) \tag{2}$$

A discrete space-time separable CIR (3), which is originally proposed by (15) and developed by (16), is employed in (17) to represent the UWB channel's impulse response. In this model, the impulse response for the multipath delay τ, so-called Time-of-Arrival (TOA), and AOA θ is given by

$$h(\tau, \theta) = \sum_{l=0}^{\infty} \sum_{k=0}^{\infty} \beta_{kl} e^{j\phi_{kl}} \delta(\tau - T_l - \tau_{kl}) \delta(\theta - \Theta_l - \omega_{kl}) \tag{3}$$

where β_{kl}, ϕ_{kl}, τ_{kl}, and ω_{kl} are respectively the amplitude, the phase shift, the arrival time and the azimuth AOA of the kth arrival of the lth cluster. T_l and Θ_l represent the lth cluster's first arrival time and the azimuth AOA respectively. In other words, for a particular cluster l the inner sum reveals the rays corresponding to the same cluster, i.e. intra-cluster representation. Accordingly, the intra-cluster rays are said to be from different ls.

3. Measurement settings

3.1 Measurement environments

UWB channel fading depends on detailed aspects of the indoor setting- including not only describing the architectural floor plan but details of the interior door. In an accurate fading study among the measurement campaigns all of these detail must be taken into account. In the present work's survey character on the indoor setting, we however consider an abbreviation but unified of the whole setting used in the measurement campaigns. Although this issue can lead to apparent wide variability in empirical results for nominally comparable setting, as more measurements are carried out new categories may be introduced which may provide a better classification in terms of the variability of the signal statistics. Table 1 represents the proposed categories based on the reviewed literature UWB channel-fading measurements.

3.2 Multipath propagation measurements techniques

Due to the importance of the multipath structure in determining the small-scale fading effects, a number of wideband channel sounding techniques have been developed. Wideband measurement techniques as described in (13) are

- *Direct Pulse (DP):* In the this measurement system, a repetitive wideband pulse is transmitted and a receiver with wide bandpass filter is utilized to receive the pulses. Then, the received signal is amplified using a Low Noise Amplifies (LNA) and detected with an envelope detector before being stored and displayed on a digital oscilloscope. This structure gives an immediate measurement of the square of CIR convolved with the probing pulse. In this measurement, the minimum resolvable delay between multipath

component equals the probing pulse width. To measure impulse response (2), the probing pulse $p(t)$ approximates the delta function. If $p(t)$ has a time duration much smaller than the impulse response of multipath channel $p(t)$ does not need to be deconvolved from the received signal in order to determine the relative multipath signal strength in the impulse response (2) (13).

- *Spread Spectrum Sliding Correlator (SC):* In a spread spectrum channel sounder, a carrier signal by mixing with a binary Pseudo-Noise (PN) sequence becomes spread over a large bandwidth and then is transmitted. The spread spectrum signal is then received, filtered and despread using a PN sequence generator. In this measurement system, the chip rate of the PN sequence generator determines the time resolution. The sliding correlator operation serves to time dilate the measured channel impulse response, thereby compressing the measurement bandwidth and easing hardware requirements. Moreover, a spread spectrum channel sounder has a higher dynamic range compared to the direct pulse system (13).
- *Frequency Sweeping (FS):* In this measurement, a Vector Network Analyzer (VNA) controls a synthesized frequency sweeper. The sweeper scans a particular frequency band by stepping through discrete frequencies. Obviously, the number and spacings of these frequency steps impact the time resolution. This frequency domain representation is then converted to the time domain using Inverse Discrete Fourier Transform (IDFT) processing, giving a band-limited version of the impulse response.

Table 1 shows what type of measurement technique is employed for the reviewed literature of the UWB channel-fading campaigns.

3.3 Space and time resolution

All above utilized measurement approaches use a band-limited probing waveform and thus have limited time resolution. Even with the sub-nanosecond resolution, used in the measurements, the received signal pulse may still contain several multipath components and thus may fade in a small local area. The time resolution can directly affect time of arrival measurements. For instance, increasing the time-domain resolution of the channel response to resolve the direct LOS path improves the performance of location finding systems employing TOA estimation techniques. Various measurement campaign's temporal resolutions are summarized in Table 1. In these measurements, the different spatial grids in size and spacing are utilized to assess the spatial variation (Table 1). The associated grids are located horizontally where the measurements are made at the center of each grid cell. Although the essential spatial fading statistics have been drawn based on the measurements made inside the grid, some campaigns like in (38) move the grid to obtain the extra parameter statistics like multipath cluster phenomenon.

3.4 Frequency range and bandwidth

A UWB signal defined by the Federal Communication Commission (FCC) is a signal with greater than 25% relative (coherent) bandwidth[1], it is also true that UWB signals tend to have large absolute bandwidths (75) which are not less than $500MHz$.
The relative bandwidth definition of UWB is stated as follows:

$$B_{rel} = 2 \cdot \frac{f_h - f_l}{f_h + f_l} = \frac{W}{f_c} \tag{4}$$

[1] Sometimes termed "fractional bandwidth".

References	Environment	Measur. Tech.	Time Res.* (ns)	Measurement Grid		Frequency-Bandwidth	
				Grid Size	Spacing (cm)	Absolute (GHz)	Relative
(17)-(23)	Office and Laboratory	DP	2	7×7	15	NA	NA
(24)-(25)	Office building and Corridor	FS	400	3×3	3	$1 - 9$	1.6
(26)	Ship Compartments	SC	NA	NA	NA	$0.8 - 2.5$	1.03
(27)-(32)	Residential House	FS	320	5×5	5	$4.375 - 5.625$	0.25
(33)-(34)	Residential and Commercial Building	FS	266.6	5×5	5	$2 - 8$	1.2
(35)	Office and Laboratory	FS	266.6	NA	NA	$2 - 8$	1.2
(36)	Residential House	FS	NA	1×20	1.253	$2 - 8$	1.2
(37)	Laboratory	FS	400	10×10	10	$2 - 6$	1
(38)	Office and Corridor	FS	NA	30×30	1	$1 - 11$	1.66
(39)	Office	FS	NA	30×30	1	$1 - 11$	1.66
(40)	Auditorium and Office	DP/SC/FC	NA	NA	NA	$1 - 3$	1
(41)-(43)	Office	SC	200	NA	NA	$1.25 - 2.75$	0.75
(44)	Office	FS	106	NA	NA	$3.1 - 10.6$	1.1
(45)	Office, Laboratory and Reading room	DP	2	1×61	2	NA	NA
(46)-(47)	Laboratory and Classroom	FS	200	NA	NA	$2 - 6$	1
(48)-(49)	Office and Classroom	DP	0.1	3×3	45	$0.1 - 12$	1.967
(50)-(51)	Office and Classroom	FS	33.6	3×3	45	$0.1 - 12$	1.967
(52)-(53)	Office	FS	500	1×90 (Circle)	2.8	$3.1 - 10.6$	1.094
(54)	Office	FS	NA	1×5	10	$3.1 - 10.6$	1.094
(55)	Office	DP	0.05	1×23	5	$3.1 - 10.6$	1.094
(56)-(58)	Office and Laboratory	SC	0.8	25×25	2	$3.6 - 6$	0.5
(59)	Office and Laboratory	FS	200	5×5	2, 8, 16	$2 - 12$	1.43
(60)	Office and Laboratory	SC	0.83	5×5	2, 8, 16	$3.6 - 6$	0.5
(61)	Residential Apartment	FS	229.6	5×5	15	$3 - 10$	1.077
(62)	Office, Laboratory, and Classroom	FS	33.6	3×3	45	$0.1 - 12$	1.967
(63)	Office, Laboratory, Factory and Residential	FS	1000	NA	100	$3 - 8$	0.91
(64)	Office	FS	100	4×4	30	$3 - 11$	1.14
(65)	MRI	DP	0.8	1×8 (Circle)	15	$3.168 - 4.752$	0.4
(66)	Office	FS	200	21×21	2	$2 - 10$	1.33
(67)-(69)	Underground Mine	FS	533	8×5	7	$2 - 5$	0.857
(70)	Underground Mine	SC	2.25	7×7	15	$2.55 - 3.45$	0.3
(71)	Office	FC	533.3	7×7	5	$3 - 6$	0.66
(72)	Office, residential, Chamber	FC	533.3	1×9	15	$3 - 6$	0.66
(73)	Chamber	FC	NA	NA	NA	$1.5 - 8$	1.368
(74)	Office and Chamber	SC	213.3	1×12 (Circle)	8	$3.1 - 10.6$	10.94

* Pulse-width for DP, twice a chip period for SC and maximum-detectable-delay for FS (13).

Table 1. UWB Channel-Fading Measurement Settings

where f_h and f_l denote frequencies at the upper and lower band edges, respectively. W is the absolute-bandwidth, and f_c is the center frequency. Table 1 shows the absolute- and relative-bandwidth utilized by each reference.

4. Channel fading's power-loss characteristics

4.1 Path-loss

Generally speaking, PL arises from the propagating wavefront's increasing surface area as the wavefront radiates outward from the transmitting antenna and the obstructive effects of objects distributed between transmitter and receiver antennas such as *free space loss*, *refraction*, *reflection*, *diffraction*, *clutter*, *aperture-medium coupling loss*, and *absorption*.

Both non-empirical and empirical propagation models illustrate that average path-loss increases logarithmically as a function of Transmitter-Receiver (TR) separation distance in

indoor radio channels (13):

$$\overline{PL\,(d)} = \overline{PL_0} + 10\,n\,\log_{10}\left(\frac{d}{d_0}\right) + F_A \tag{5}$$

where n, PL_0, d and F_A are respectively the path-loss exponent which shows the rate at which the path-loss increases with distance, the intercept point which is the path-loss at d_0 (a reference distance), the transmitter-receiver separation distance, and the Floor Attenuation Factor (FAF). The bars in (5) denote the average values for the same floor measurement and over all transmitter-receiver antennas locations, while maintaining the same transmitter-receiver separation distance. The variations about the average path-loss value (5) are called shadow fading and are discussed later. The path-loss exponent n depends on the propagation environment. In free space, $n = 2$; with obstructions, $n > 2$ (13).
Measurements (21), (22), (24)-(27), (29), (30), (33), (34), (41)-(43), (45)-(58), (60), (63), (65), (68), (70)-(72) and (74) show that (5) is applicable for both Line-of-Sight (LOS) and Non-Line-of-Sight (NLOS), i.e. when there is no LOS path between the transmitter and receiver, UWB channels with the calibrated PL parameters in Table 2. Depending on the UWB receiver architecture, the PL parameters can be obtained by different methods. Basically, the UWB indoor path-loss is calculated by the total received power integrating the power delay profiles (defined in 5.2.1) over all delay bins (21), (22), and (41)-(43). However, if the receiver uses a threshold detection strategy which tracks the peak of the received signal, the calculated PL is based on the peak CIR power metric (41)-(43). Moreover, some of the receiver structures only detect the first path; thus, the first path power is only employed for the PL calculation (63).
The UWB indoor path-loss exponent n measured in different environments behaves as a random variable (24), (25), (27), (29) and (30). In (27), (29), (30), (33) and (34), it is also shown that n follows a normal distribution (see Table 2). From the measurement results:

1) Table 2 shows $1.4 < n < 4.1$ for a regular indoor environment except for the hard-NLOS situation (22), (60) and (63), and a very short-distance path-loss measurements (55) and (65). A hard-NLOS scenario is basically defined for when there is no direct or reflected path between transmitter and receiver e.g. two different rooms (24). However, in (60) this definition corresponds to the situation in which not only the transmitter and receiver are located in different rooms but also the blockage effect of the other obstacles are considered. On the other hand, a soft-NLOS scenario mostly happens when there are reflected paths between the transmitter and the receiver. e.g. in a room. In (22) and (60), the high value path-loss exponent $n = 7.4$ is reported for a multi-wall scenario. Moreover, $n = 4.9$ is reported in (63) for a multi-floor measurement. In (55) and (65), it is shown that for a short distance NLOS scenario the path-loss exponent n is less than 1. This result, however, can be justified using a small scale fading. The path-loss exponent for a
2) It is shown in (22) and (63) that the path-loss exponent n can be dependent on the TR distance. To present this dependence, a *dual-slope* model of the normalized mean PL (5) is proposed in (22) and (63) for different distance regions

$$\overline{PL_D\,(d)} = \begin{cases} 10\,n_1 \log_{10}\left(\frac{d}{d_0}\right) & d \le D \\ \overline{PL_D} + 10\,n_2 \log_{10}\left(\frac{d}{d_0}\right) & d > D \end{cases} \tag{6}$$

References	Environment		d_0 (m)	$\overline{PL_0}$ (dB)	n^*		$\sigma_\chi(dB)$		Notes
					μ_n	σ_n	μ_{σ_χ}	σ_{σ_χ}	
(21)	Office/Laboratory	LOS/NLOS	1	NA	2.4	NA	5.9	NA	-
(22)	Office/Laboratory	LOS/NLOS	1	$0^\dagger$	2.04	NA	4.3	NA	$d \leq 11m$
				$-56^\dagger$	7.4	NA			$d > 11m$
(24)-(25)	Office	LOS	0.151	39.82	1.4	0.35	NA		-
		Soft-NLOS	0.082	NA	3.2	0.21			
		Hard-NLOS	0.067	NA	4.1	1.87			
(26)	ship Compartment	NLOS	NA	NA	1.65	NA	NA		-
(27), (29)-(30)	Residential	LOS	1	47	1.7	0.3	1.6	0.5	-
		NLOS	1	51	3.5	0.97	2.7	0.98	
(33)-(34)	Commercial	LOS	1	43.7	2.04	0.30	1.2	0.6	-
		NLOS	1	47.3	2.94	0.61	2.4	1.3	
	Residential	LOS	1	74.2	1.82	0.39	1.5	0.6	
		NLOS	1	50.4	3.34	0.73	2.6	0.9	
(42)-(43)	Office	NLOS	1	$0^\dagger$	3	NA	NA		Peak Power, $d > 1m$
					2	NA			Total Power
(41)	Office	NLOS	NA	NA	2.9	4.75	NA		Peak Power
					2.1	3.55			Total
(45)	Office/Laboratory	LOS/NLOS	1	$-10.9^\dagger$	3.4	NA	3.2	NA	$d > 5m$
	Reading room	LOS	1	$1.15^\dagger$	1.8	NA	0.6	NA	
(46)-(47)	Laboratory/ Classroom	LOS	1	NA	1.55	NA	1.98	NA	{RX,TX}={OMNI,OMNI}
					1.65	NA	1.19	NA	{RX,TX}={OMNI,DIR}
					1.72	NA	0.77	NA	{RX,TX}={DIR,DIR}
(48)-(49)	Office/Classroom	LOS	1	NA	1.58	NA	1.91	NA	Biconical Antenna
		NLOS	1	NA	2.41	NA	3.26	NA	
		LOS	1	NA	1.6	NA	1.58	NA	TEM Horn Antenna
		NLOS	1	NA	2.6	NA	6.08	NA	
(50)-(51)	Office/Classroom	LOS	1	NA	1.3	NA	2.6	NA	Biconical Antenna
		NLOS	1	NA	2.3	NA	2.4	NA	
		LOS	1	NA	1.3	NA	2.8	NA	TEM Horn Antenna
		NLOS	1	NA	2.4	NA	5.1	NA	
(52)-(53)	Office	LOS	1	53.7	1.62	NA	1.7	NA	-
		NLOS	1	59.4	3.22	NA	5.7	NA	
(54)	Office	LOS	0.1	4	1.7	NA	NA	NA	-
(55)	Office	LOS	1	20	2.21	NA	NA	NA	RX & TX on a desk
		NLOS	1	20	-1.06	NA	NA	NA	Monitor Blocked
				NA	1	NA	NA	NA	Desk Blocked (on & under)
				7.5	0.17	NA	NA	NA	Body Blocked
(56)-(58)	Office/Laboratory	LOS	1	50.54	1.916	NA	1.42	NA	-
		NLOS	3.73	67.15	3.663	NA	2.18	NA	
(60)	Office/Laboratory	LOS	1	NA	1.8	NA	2.57	NA	-
		NLOS	4.037	NA	11.05	NA	5.17	NA	
		Hard-NLOS[2]	4.037	NA	7.33	NA	NA	NA	Multi-wall effect
(63)	Office/Laboratory	Hard-NLOS	1	42	3.5	NA	5.1	NA	$d \leq 10m$
				77	2.2	NA			$d > 10m$
	Residential	NLOS		42	2.7	NA	3.9	NA	Same floor
					3.6	NA	2.7	NA	Inter-floor
	Factory	LOS		42	1.5	NA	2.4	NA	$d \leq 10m$
				57	2.9	NA			$d > 10m$
(65)	MRI	LOS/NLOS	0.087	28	0.435	NA	NA	NA	Empty barrel
					0.646	NA	NA	NA	Water-filled barrel
(67)-(69)	Underground Mine	LOS	1	66	1.47	NA	1.1	NA	-
		NLOS	5	52.5	2.45	NA	2.94	NA	
(70)	Underground Mine	LOS/NLOS	10	$0^\dagger$	1.8	NA	NA		Peak Power
					1.64	NA			Total Power
(71)	Office	LOS/NLOS	0.1	56.1	5.8	NA	5	NA	-
(72)	Office	NLOS	1	75.8	2.67	NA	NA	NA	-
	Chamber	LOS	1	82	3.29	NA	NA	NA	
(74)	Office and Chamber	LOS/NLOS	1	82	2.6	NA	NA	NA	-

* The same-floor path-loss exponent (see note for some exceptions).

† These intercept values are calculated based on a normalized path-loss.

Table 2. Path-loss Characteristics

where D, $\overline{PL_D}$, n_1 and n_2 are respectively the break point distance in the model, the intercept point, the path-loss exponent for the first slope, i.e. $d \leq D$, and the path-loss exponent for the second slope, i.e. $d > D$. All these values are calculated through the curve-fitting process on the measured data.

3) There is no significant difference between the measured values of n for UWB channels and narrowband indoor channels which are reported in (13).
4) The path-loss in a ship compartment area follows in-building LOS (within one room) cases.
5) The path-loss exponent n slightly increases if directional antennas are employed for the receiver and transmitter (46)-(51) because it reduces some of the obstructive effects of objects distributed between transmitter and receiver like diffraction, reflection and absorption. In other words, the directive antenna does not use the considerable multipath energy while an omni-directional antenna does.
6) The standard deviation of the path-loss exponents for different measurement locations/environments, like rooms and buildings but in the same category like residential (27), (29) and (30), is higher for NLOS cases than for LOS cases.
7) Different types of indoor environment (e.g. office, laboratory, residences) lie in different subranges of $n \in [1.4, 4.1]$. Instead of a deterministic n, it has been modeled as a Gaussian random variable with empirically determined mean and variance, for residential houses in (27), (29) and (30), and commercial areas in (33) and (34).
8) To the best of the authors' knowledge, there is only one published paper on the F_A measurement (63). It is shown in (63) that there is no significant difference in the path loss model between a single and multi-floor measurement. However, the results in (63) show a considerable difference between the aforementioned scenarios when the measurements are performed at the entrance/back of the building.

4.2 Large-scale fading

(5) overlooks shadowing loss (χ), which augments (5) to:

$$PL(d) = \overline{PL(d)} + \chi \tag{7}$$

UWB measurements (21), (22), (24), (27), (29), (30), (33), (34), (41), (43), (45)-(53), (56)-(58), (60), (63) and (68) indicate a zero-mean log-normally distribution for χ with its standard deviation σ_χ dependent on the particular propagation environment (see Table 2). >From large-scale fading measurement results:

1) Shadowing loss is generally greater for residences than for offices. environments.
2) In a LOS scenario, the shadowing loss is less than in a NLOS case.
3) For the LOS scenarios, the shadowing loss decreases if directional antennas are employed for the receiver or transmitter. Indeed, the spatial filtering using a directive antenna results in a more stable average PL.
4) To the authors' knowledge, there are no published paper investigating the relationship between χ and the transmitter-receiver separation distance, there exists only one paper published on the inter-floor shadowing loss (63) which reports an inter-floor shadowing loss less than the same-floor shadowing loss for a residential environment (see Table 2). The same result is also observed for an office/laboratory environment (the inter-floor

References	Environment		Small-Scale Type	distribution(s)**	distribution parameters
(17)	Office/Laboratory	LOS/NLOS	Spatial	Rayleigh(σ)	$\sigma = 0.46$
(21)- (22)	Office/Laboratory	LOS/NLOS	Spatial	Nakagami(m)	$m \sim \mathcal{N}[\mu_m(\tau_k), \sigma_m^2(\tau_k)]$
(24) and (25)	Office/ Laboratory/ Corridor	LOS	Temporal	Weibull(μ, σ, λ)	$\mu = -306, \sigma = 311, \lambda = 45$
		Soft-NLOS			$\mu = -304, \sigma = 320, \lambda = 46$
		Hard-NLOS			$\mu = -304, \sigma = 322, \lambda = 45$
(31)	Residential	LOS/NLOS	Temporal	Gaussian($0, \sigma$)	$\sigma = 4.7$
(35)	Office/Laboratory	LOS	Temporal	Rician(k)	$k \propto \{d^*, \tau_k\}$
(38)	Office/Corridor	LOS/NLOS	Temporal	Rician(k)	$k = -9dB$
(39)	Office	NLOS	space-time‡	Gaussian($0, \sigma$)$\times$ Potential(a)	NA
(45)	Office/Laboratory	LOS/NLOS	Spatial	Gaussian($0, \sigma$)	$\sigma_{d^*=5} = 1.13, \sigma_{d=7} = 1.24$ $\sigma_{d=10} = 1.16, \sigma_{d=14} = 1.41$
	Reading room	LOS			$\sigma_{d=5} = 0.13, \sigma_{d=7} = 0.26$ $\sigma_{d=10} = 0.22, \sigma_{d=14} = 0.31$
(52)	Office	LOS/NLOS	Spatial	Rician(k)	NA
(57)	Office/Laboratory	LOS/NLOS	Spatial	Nakagami(m)	$\mu_m = 1.5, \sigma_m = 0.5$
(71)	Office	LOS/NLOS	Spatial	Nakagami(m)	Corresponding αGamma=2

* d is the transmitter/receiver separation distance.
** All distributions are on amplitude except Weibull(μ, σ, λ) which is for received power.
‡ The Gaussian distribution corresponds to the spatial small-scale amplitude and the Potential distribution corresponds to the temporal small-scale amplitude.

Table 3. Small-scale statistics

shadowing loss $\sigma_\chi = 1.8$ and the same-floor shadowing loss $\sigma_\chi = 3.4$) (63). However, in such an environment when we move from the inter-floor scenario to the multi-floor one the inter-floor shadowing loss increases even more than a same-floor case (the inter-floor shadowing loss $\sigma_\chi = 1.8$ and the multi-floor shadowing loss $\sigma_\chi = 5.1$) (63).

5) As many wireless devices are wearable, the human-antenna interaction could be significant not only in open areas (40) but also in dense scatterer environments (like in an office) (71). A UWB channel measurement for Body Area Networks (BAN) is presented in (72). Significant echoes from the body, e.g. from the arms, and deterministic echoes from the floor are observed in human-body effect measurement (72). In (74), the performance of the UWB impulse radio for BAN employing a monopole antenna. The results in (74) show that the shadowing loss in a WBAN channel does not follow the log-normal distribution. Obayashi and Zander (77) model the body-shadowing deterministically with the existing ray-determination methods for narrow-band channels, but no corresponding study has been done for UWB with UWB's distinctive demands on ray-tracing methods.

4.3 Small-scale fading

Basically, "small-scale fading" describes the received signal amplitude/energy's fluctuations over a short duration or in the spatial neighborhood at the moving antenna's nominal location (13). This definition can be generalized to UWB communications as the constructive and destructive interferences of the multipath components due to a change in the moving antenna location in the order of the sub-spatial width of the transmitted pulse. In the UWB small-scale measurements, the moving antenna is mostly receiver antenna (17), (21), (22), (24), (25), (31), (35), (39), (45), (57) and (71); however, a moving transmitter antenna is used in (38) and (52). In the UWB indoor applications, the transmitter an receiver and scatterer move slowly (if at all) relative to the information symbol duration. The UWB channel's small-scale fading thus depends mostly on the multipath phenomena and the signal bandwidth.
Measurement campaigns (17), (18), (21), (22), (24), (25), (31), (35), (38), (39), (45), (52), (57) and (71) present different results for the small-scale statistics of received signal amplitude/energy due to *measuring time-delay interval*, *measuring data set (grid size and spacing)*, and *environment type*. Table 3 shows the proposed mathematical distributions, associated with the measured

essential parameters (shown in the last column), for the small scale fading reported by different measurement campaigns. >From small-scale fading measurement results:

1. The small-scale distribution's parameters depend on the transmitter-receiver separation distance.
2. Most of the small-scale amplitude measurements show the clustering effect.
3. The more clustered office environment generally has higher standard deviations than open areas like reading rooms, due to the multipath phenomenon.
4. The small-scale distribution strongly depends on environment type (e.g. it is shown in (39) that the small-scale amplitude follows the Gaussian distribution whose parameters are fixed for an European office, and also results from (21) and (22) show that the small-scale amplitude follows the Nakagami distribution whose parameters change with increasing excess delay for an American office).
5. As each temporal bin sums many multipath, the central limit theorem gives the Gaussian distribution for the small-scale magnitude statistics for large delays, but the Gaussian distribution is only approximate at small delays; hence, the Nakagami distribution (21) and (22) whose parameters change with increasing excess delay can fit well the small-scale amplitude while the Gaussian distribution is proposed in (7) for mathematical convenience.

5. Channel fading's temporal characterizations

5.1 Multipath arrival rate

The arrival rate model in (16) is employed in (17), (52) and (57) to measure arrival rate statistics based on the multipath clustering phenomenon used in (3)

$$p\left(T_l|T_{l-1}\right) = \Lambda e^{-\Lambda\left(T_l - T_{l-1}\right)} \tag{8}$$

$$p\left(\tau_{k,l}|\tau_{(k-1),l}\right) = \lambda e^{-\lambda\left(\tau_{k,l} - \tau_{(k-1),l}\right)} \tag{9}$$

where Λ and λ are respectively the cluster arrival rate and the ray arrival rate. Results in (17), (52) and (57) show a smaller ray-arrival rate but a larger cluster-arrival rate for UWB than in (16) for narrowband (see Table 4). Due to UWB's smaller ray-arrival rate but a larger cluster-arrival rate than narrowband, the reflection mechanism seems to be superior than other mechanisms like diffraction. In (71), a different model is suggested for BAN channels. Indeed, it is shown in (71) that a Weibull distribution provides a better fit to the measured data for the arrival rate statistics.

5.2 Multipath delay spread

5.2.1 Power delay profile

"power delay profile" is the small-scale averaged Instantaneous Power Delay Profile (IPDP) $P(\tau) = |h(\tau)|^2$ (13) where $h(\tau)$ is the multipath CIR defined in (2). The average IPDP is made over a local area (a neighborhood at the moving antenna's nominal location) for spatial small-scale or over a short period of time (mostly a delay resolution *bin*) for temporal small-scale. As shown in (17), (21), (22), (24), (25), (28), (31), (37), (38), (52) and (57), the power delay profile is related to the excess delay as

$$\overline{P\left(\tau\right)} = \overline{a_0^2}\, e^{-\frac{\tau}{\gamma}} \tag{10}$$

Parameters	UWB (17)	UWB (52)		UWB (57)		Narrowband (16)	Narrowband (16)
		LOS	NLOS	LOS	NLOS	(*Building 1*)	(*Building 2*)
$\frac{1}{\Lambda}$	45.5	27.4	40.1	39	17	16.8	17.3
$\frac{1}{\lambda}$	2.3	0.168	0.161	NA	NA	5.1	6.6
Γ_C	27.9	15.7	7.5	25.18	13	33.6	78.0
γ_r	84.1	16.5	12	12.2	18	28.6	82.2

Table 4. Narrowband and UWB Propagation Channels' Arrival Rates and Time Constants (ns)

where $\overline{a_0^2}$ denotes the first multipath's average power and γ symbolized power decay-rate. Moreover, the presented data in (17), (52) and (57) verify the double exponential decay law of (15):

$$\overline{P\left(T_l, \tau_{kl}\right)} = \overline{a_0^2} \cdot e^{-\frac{T_l}{\Gamma_C}} \cdot e^{-\frac{\tau_{kl}}{\gamma_r}} \tag{11}$$

where Γ_C and γ_r determine the inter-cluster (i.e. the earliest arrival of each cluster) decay-rate and the intra-cluster (i.e. arrival rays inside the clusters) decay-rate, respectively. The parameters Γ_C and γ_r are measured in (17), (52) and (57) via a manually, so-called visually-inspection, cluster selecting approach. Moreover, it is shown in (71) that a linear-exponential decay law could fit the measurement results better than the double-exponential one. In (71), a dual-slope model is suggested for the cluster arrival time and an exponential model for the ray arrival time. Table 5 summarizes the power delay profile empirical statistics presented in the open literature. From the UWB's power delay profile measurement results:

1. Referring to the double exponential model (11), UWB has smaller inter-cluster decay-rate comparing to narrowband (see Table 4). However, different results provided in (17), (52) and (57) do not show any trend comparing with the narrowband measurement (16). In fact, these parameter highly depend on the particular propagation channel setting. For instance, the inter-cluster decay-rate depends primarily on the building and the floor-plan itself but the intra-cluster decay-rate depends primarily on furnishing.
2. Measurements always have decreasing power decay-rate mean and standard deviation with more obstruction.
3. The delay profile's attenuation is inversely proportionate to the transmitter-receiver separation distance.
4. Reflection gives the strongest paths in power delay profile with a noticeable difference than other multipath mechanisms like diffraction; hence, other mechanisms such diffraction and diffuse scattering are minor and ignorable. Corridors, due to their LOS nature and unlike offices, have two clusters. The minor-cluster is a copy of the main-cluster, reflected off the opposite wall. Hence, the main-cluster's delay is inversely proportional to the transmitter-receiver separation distance.

5.2.2 Time dispersion

Time dispersion phenomenon, mainly due to multipath in an indoor propagation environment, can highly affect the transmitted data rate and reduce the capacity in a multi-user UWB communication system. The time dispersion of the UWB signals is usually presented by the first central moment and the square root of the second central moment of

Reference	Environment		$\overline{a_0^2}$	γ (ns)		τ_{RMS} (ns)		Notes
				Mean*	σ_γ	Mean*	σ_τ	
(17)	Residential	LOS/NLOS	0.2	28	NA	NA	NA	inter-cluster arrivals
			0.3	84	NA	NA	NA	intra-cluster arrivals
(21)-(22)	Office/Laboratory	LOS/NLOS	0.031	39.8	1.34	NA	NA	-
(24)-(25)	Office/Laboratory/ Corridor	LOS	NA	0.010	0.021	NA	NA	$\frac{1}{\gamma}$ statistics
		Soft-NLOS	NA	0.008	0.018	NA	NA	
		Hard-NLOS	NA	0.006	0.023	NA	NA	
(26)	ship compartment	NLOS	NA	NA	NA	82.6	NA	-
(27)	Residential	LOS	NA	NA	NA	4.7	2.3	-
		NLOS	NA	NA	NA	8.2	3.3	
(28)	Residential	LOS	0.23	0.83	1.06	NA	NA	$\frac{1}{\gamma}$ statistics
		NLOS	NA	0.89	1.03	NA	NA	
(31)	Residential	LOS	0.4	1.09	0.14	4.56	2.16	$\frac{1}{\gamma}$ statistics $d^\dagger = 5m$
		NLOS	0.1	1.07	0.12	8.98	4.23	
(37)	Laboratory	LOS	NA	34.36	2.16	12.3	0.5	$d = 5m$
		NLOS	NA	43.77	1.96	14.86	1.65	
(38)	Office	LOS/NLOS	NA	13.6	1.5	NA	NA	-
(41)	Office	NLOS	NA	NA	NA	6	5.22	$d = 5m$
(42)	office	NLOS	NA	NA	NA	20	NA	$d = 5m$
(45)	Office/Laboratory	LOS/NLOS	NA	NA	NA	14.3	2.8	-
	Reading Room	LOS	NA	NA	NA	19.9	1.8	
(46)-(47)	Laboratory/ Reading Room	LOS	NA	NA	NA	17.34	NA	{RX,TX}={OMNI,OMNI}
			NA	NA	NA	11.35	NA	{RX,TX}={OMNI,DIR}
			NA	NA	NA	7.71	NA	{RX,TX}={DIR,DIR}
(48)-(49)	Office/Classroom	LOS	NA	NA	NA	7	5	Biconical Antenna
		NLOS	NA	NA	NA	13	7	
		LOS	NA	NA	NA	3	2	TEM Horn Antenna
		NLOS	NA	NA	NA	10	5	
(50)-(51)	Office/Classroom	LOS	NA	NA	NA	8.5	NA	Biconical Antenna
		NLOS	NA	NA	NA	16.2	NA	
		LOS	NA	NA	NA	1.7	NA	TEM Horn Antenna
		NLOS	NA	NA	NA	7.1	NA	
(52)-(53)	Office	LOS	NA	15.7	NA	4.1	2.7	inter-cluster arrivals
		NLOS	NA	16.5	NA	9.9	5	
		LOS	NA	7.5	NA	4.1	2.7	intra-cluster arrivals
		NLOS	NA	12	NA	9.9	5	
(55)	Office	LOS	NA	NA	NA	6.6	NA	-
		NLOS	NA	NA	NA	9.3	NA	
(61)	Residential	LOS	NA	NA	NA	14	1	-
		NLOS	NA	NA	NA	35	6	
(64)	office	NLOS	NA	NA	NA	22.8	2.61	-
(65)	MRI	LOS/NLOS	NA	NA	NA	12	NA	Empty barrel
			NA	NA	NA	5	NA	Water-filled barrel
(68)	Underground Mine	LOS	NA	NA	NA	11.8	4.4	-
(70)	Underground Mine	LOS	NA	NA	NA	34	NA	-
		NLOS	NA	NA	NA	42	NA	
(72)	Office	NLOS	NA	NA	NA	3.2	NA	-
	Chamber	LOS	NA	NA	NA	1.5	NA	
(73)	Chamber	LOS	NA	NA	NA	1.5	NA	-
(74)	Office and Chamber	LOS/NLOS	NA	NA	NA	< 12	NA	-

* over all measurement
† d is the transmitter/receiver separation distance

Table 5. Multipath Delay Spread Statistics

PDP, i.e. the mean excess delay τ_m and the root mean square delay spread τ_{RMS}, defined as follows

$$\tau_{RMS} = \sqrt{\frac{\sum_i \overline{P(\tau_i)}\,(\tau_i - \tau_m)^2}{\sum_i \overline{P(\tau_i)}}}, \quad \tau_m = \frac{\sum_i \overline{P(\tau_i)}\tau_i}{\sum_i \overline{P(\tau_i)}} \tag{12}$$

Strong echoes with long delays contribute disproportionately to τ_{RMS} which is provided to communications performance. Most of the measurement campaigns employs the delay spread τ_{RMS} to evaluate the time dispersion of the UWB pulses. However, the ratio τ_m / τ_{RMS} is also suggested in (48), (49) and (58) as an effective criterion of the time dispersion. The delay spread τ_{RMS} is empirically found to depend on the environment structure such as the size and type of building and existence or absence of a clear LOS path (Table 5). UWB measurements (27), (37), (41)-(43), (46), (47) and (65) show that τ_{RMS} increases with increasing the transmitter-receiver separation distance. A Normal distribution is suggested by (27), (28), (31) and (45) to approximately fit the τ_{RMS} variations. Since both path-loss and τ_{RMS} increase with transmitter-receiver separation, a correlation between them can be investigated. It is shown in (27), (41) and (65) that the path-loss increases linearly as τ_{RMS} goes up. Moreover, the delay spread τ_{RMS} is more correlated with path-loss than with the transmitter-receiver separation, for offices. To summarize, the delay spread τ_{RMS}

1) is directly related to the transmitter-receiver separation.
2) has a higher mean and standard deviation for LOS than for NLOS.
3) is log-normal for office, laboratory, reading room and residential areas where office/laboratory and reading room have the same standard deviation as residence NLOS and LOS cases respectively.
4) is decreased when the antenna becomes more directive.
5) is more correlated with path-loss than with the transmitter-receiver separation for offices.

5.3 Temporal correlation

The temporal correlation coefficient is computed by spatially averaging the correlation between the power of the multipath components arriving to the same room at different excess delays.

$$\rho_{i,i+l} = \frac{E\left\{\left(P(\tau_i) - \overline{P(\tau_i)}\right)\left(P(\tau_{i+l}) - \overline{P(\tau_{i+l})}\right)\right\}}{\sqrt{E\left\{\left(P(\tau_i) - \overline{P(\tau_i)}\right)^2\right\} E\left\{\left(P(\tau_{i+l}) - \overline{P(\tau_{i+l})}\right)^2\right\}}} \tag{13}$$

where $E\{.\}$ denotes the spatial averaging over the local area. The temporal correlation coefficient $\rho_{i,i+l}$ is useful metric to reveal the resolvability of the CIR components in the impulse radio channels, i.e. UWB. It is enough to calculate the correlation coefficient between adjunct bins as this coefficient obviously decreases when the bins are in distance on the time axes.

Measurements (21), (22) and (45) show that the temporal correlation coefficient is below 0.2 and negligible for indoor UWB. This results in a resolvable fading for the UWB channels and benefits of using RAKE receivers for this kind of channels.

Parameters	UWB (36)	UWB (17)	NB (16) (*Building 1*)	NB (16) (*Building 2*)
σ	22.5°	38°	25.5°	21.5°

Table 6. Azimuth AOA Standard Deviation

6. Channel fading's spatial characteristics

6.1 The fading multipath angle of arrival

Obstacles like walls, floor, furniture and human-body throughout a building, causes AOA to spread over a wide range and frequency-dependent due to frequency-dependent reflection, scattering and/or diffraction (87). Welch *et al.* (40) present measurements that for open-areas (like auditorium) antenna-human intracts to create a very sharp null, but little effects for highly clustered environments (like office). Prettie *et al.* (36) show the signal's AOA is frequency-independent for LOS, but frequency-dependent for NLOS case. (36) gives a smaller range of the signal's AOA for residence than in (17) for offices (Table 6).
Cramer *et al.* (17) assume CIR (3) to be separable function of delay and azimuth: $h(\tau,\theta) = h_1(\tau)h_2(\theta)$ where $h_2(\theta) = \sum_{l=0}^{\infty}\sum_{k=0}^{\infty}\beta_{k,l}\delta\left(\theta - \Theta_l - \omega_{k,l}\right)$ due to the angular deviation of the signal arrivals within a cluster from the cluster mean, over all AOA's within the cluster, does not increase as a function of delay. In (17), Θ_l is found using the above mathematical form to be approximately uniform over all angles and ω_{kl} is zero-mean Laplacian:

$$p(\omega_{kl}) = \frac{1}{\sqrt{2}\sigma}e^{-\left|\frac{\sqrt{2}\omega_{kl}}{\sigma}\right|} \tag{14}$$

with a standard deviation (σ) of 38° which is larger than for narrowband channels (Table 6). Moreover, the received signal magnitude $\beta_{k,l}$ is a Rayleigh-distributed random variable with a mean-square value which follows the double exponential (11) as $\overline{\beta_{k,l}^2} = \overline{P(T_l,\tau_{kl})}$ (17). To summarize:

1) The inter-cluster and intra-cluster azimuth AOA is uniform and Laplacian, respectively similar to narrowband (80). However, UWB has a wider ($\sigma = 38°$) Laplacian distribution for the intra-cluster azimuth AOA than narrowband.
2) AOA is frequency-independent for the LOS case but frequency-dependent for the NLOS case. Offices have wider ($\sigma = 38°$) AOA spread than household ($\sigma = 22.5°$).
3) The human-body has a little effect on AOA spread in dense environments but can create a very sharp nulls in open areas.

6.2 Received data's spatial correlation across the receiver's spatial aperture

The spatial dependence of the UWB channels is analytically demonstrated via a space-frequency correlation function between the received signals S_1 and S_2 (36)

$$R(\xi,\omega) = E\{S_1S_2\} = J_0\left(\omega\frac{\xi}{c}\right) + \frac{2}{\beta}\sum_{\substack{n=-\infty\\ n\neq 0}}^{\infty}\frac{j^n}{n}J_n\left(\omega\frac{\xi}{c}\right)e^{jn\alpha_0}\sin\left(\frac{n\beta}{2}\right) \tag{15}$$

where $J_n(.)$, ξ, c, ω, β and α_0 represent respectively the nth-order Bessel function, the inter-antennas spacing distance, the speed of light, the wireless frequency, the angular range in which AOA is assumed to be uniformly distributed and the AOA mean. As (15) implies, the correlation length is less at higher frequency. To evaluate this result, Prettie *et al.* (36) have made a set of measurements along baselines of the antenna positions at several locations in

a residential environment. Although the measurement results (36) for NLOS case obey the space-frequency correlation function (15), they contradicts (15) for LOS case. Another set of spatial correlation measurements has been reported in (45). Li and Wong (45) show that

1. The average spatial correlation coefficient to depend on the excess delay. This averaging is made over all antenna separations and over all antenna locations for each environment. The correlation reaches the highest values for $\tau = 0$, but then decreases for larger excess delay ($\tau = 10ns$).
2. For the same excess delay, the open areas like high ceiling reading room present a higher correlation coefficient than office/laboratory environments.
3. The correlation coefficients for $\tau = 0$ are insensitive to the transmitter-receiver separation in offices/laboratories.

7. Channel fading's frequency-dependent characteristics

Due to a large bandwidth in UWB systems, the *frequency-dependent* aspects of the channels should be taken into account when we characterize and model the channel. There exist many frequency-relative components of the UWB communication channel which affect the traveling signal like the antenna pattern, materials in the propagation environment etc. In such a channel, not only the frequency selectivity of the environment, which is mainly due to the propagation effects e.g. multipath phenomenon, disperses the transmitted signal but also the transmit/receive antenna does. Hence, in an impulse radio channel these aspects must be evaluated separately as are done in this section.

7.1 Frequency selectivity

7.1.1 Transfer function characterization

Obstructions situated between the transmitter-receiver behave differently as different frequencies. To account for frequency-dependent electromagnetic behavior of scatterers, (1) is generalized in (8) to:

$$h(\tau, t, f_n) = \sum_{i=0}^{N(t,f_n)-1} a_n(\tau, t, f_n)\, e^{\theta(\tau,t,f_n)} \delta(\tau - \tau_n(t, f_n))$$

where f_n is the nth operating frequency. In this model, the total bandwidth is divided into several sub-bands. The center frequency of the sub-bands is called operating frequency. Moreover, a distinct wideband model, considering the bandwidth, for each sub-band in UWB is proposed in (8). The above-mentioned frequency-dependency has been verified by the measurements in different ways. Measurements (24), (25), (36), (38), (43) and (79) show that the power gain decreases with increasing frequency; as for free-space propagation, the received power is proportional to f^{-2} (38), (42), (43), (79). Alvarez *et al.* (24), (25) show that the mean level, averaged spatially on the assigned local area (see Table 1), of channel transfer-function (in dB) is approximately :

$$10 \log_{10} \overline{|H(f)|^2} = k_p\, e^{-\delta f} \tag{16}$$

where k_p and δ are respectively a constant and the frequency decaying factor which is highly dependent on the antenna specifications (24) and (25). In (24) and (25), it is indicated that the obstruction leads to faster power-decay per unit frequency (see Table 7). Kunisch and

Cases	δ (nS)	
	$E[\delta]^*$	$\sigma[\delta]^*$
LOS	1.01	0.18
Hard-NLOS	1.16	0.21
Soft-NLOS	1.36	0.24

* over all measurements in each case

Table 7. Frequency Decaying Factor δ Statistics

Pamp (38) have also investigated the frequency-dependent power-decay in offices, for both LOS and NLOS, which includes inside office NLOS and through-wall, i.e. hard-NLOS (24), cases. This frequency dependency is first studied in 1990s by using a physics-based approach (88)-(90). The NLOS case has a slightly steeper decay than LOS case for higher frequencies. The mean transfer-function magnitude, averaged spatially on the assigned local area (see Table 1), decays with increasing frequency:

$$\overline{|H(f)|} = k_a \left(\frac{f}{F}\right)^{-m} \tag{17}$$

where $|H(f)|$, $F = \sqrt{f_h f_l}$, k_a and m, are respectively the transfer-function magnitude, the center frequency with bandwidth $BW = f_h - f_l$ (see Table 1), the amplitude factor, and the power law exponent. For the LOS case $m \sim 2$ with little variance because of the strong paths' coherent summation. However, moving from LOS to NLOS results in a a large decrease in m, i.e. a slower decay with f. For the NLOS and between-offices cases, m has larger variance as the multipath become more obstructed, but has mean equal 1.2 for the between-offices cases 1 and 2, and 1.1 for NLOS case. For both LOS and NLOS cases, $\log_{10} k_a$ is almost linear dependent on m, i.e. one can write $m = \alpha \log_{10} k_a$ where α is real positive value. Substituting this linear function into (17) yields

$$\overline{|H(f)|} = k_a \left(\frac{f}{F}\right)^{-\alpha \log_{10} k_a} \tag{18}$$

As seen $\overline{|H(f)|}$ is no longer a linear function of k_a and therefore deviates from the simple power law. Lao *et al.* (44) show how the transmission coefficients with amplitude and phase information change for different building materials. According to their investigation, the amplitude decreases slightly with increased frequency for chip-wood material whereas for other materials: plaster board, calcium-silicate board and tempered-glass, the amplitude changes randomly. Meanwhile, it is shown in (44) that the variations in the transmission coefficient amplitude for tempered-glass are significant in the measured band. Moreover, the frequency behavior of the channel based on both vertical and horizontal polarization is measured in (44). For different polarizations, measurement results indicate that variation is not significant for plaster-board and Ca-Si board. For tempered glass, the variation is large than the other material in the most of the band. To summarize:

1. $\overline{|H(f)|^2}$ decays exponentially versus frequency. More clustered obstruction increases this decay rate.
2. $\overline{|H(f)|^2}$ deviates from the power law, with m having a larger variance with more obstruction. $\log_{10} k_\beta$ is approximately linearly related to m.
3. As expected, there is a strong relationship between the frequency-dependent parameters of channel and the materials used in the propagation environments.

7.2 Pulse-distortion

7.2.1 Physical description

As shown in Section 7.1, the UWB channel is seen to be frequency-selective. The phenomenon can be apparently explained by the Geometric Theory of Diffraction (GTD) in the frequency domain. However, from the electromagnetics point of view this frequency dependence is not surprising in the high-frequency radio propagation. This frequency dependency accordingly causes the pulse distortion in the time domain.

Investigations in (81)-(89) show a true picture for the UWB radio propagation which says if a pulse propagates along multiple rays or paths, the received pulses will experience different pulse distortion for different paths. In other words, the pulse waveforms of these received pulses are different. These different pulse-distortions are basically difficult to model by the state of the art statistical measurements. Hence, the physics-based deterministic behavior of the UWB pulse transmission needs to be considered to parameterize the pulse-distortion. In particular, recently the IEEE 802.15.4a channel model (90) adopted a special form of the channel model suggested in (87), (88) and (89). It cited two papers (88) and (89) for first introducing the frequency dependence in the channel model.

Although the pulse-distortion is not so severe for indoor applications such as those targeted by IEEE 802.15.3a, it could cause serious problems for IEEE 802.15.4a systems. To address these problems, (91) and (92) give a tutorial review of physics-based ultra-wideband signals and their optimum and sub-optimum detection. Moreover, in (91) a physics-based deterministic model, which captures a lot of properties that are not available in the existing statistical models such as the IEEE 802.15.4a model, is proposed for urban environments consisting of high-rise buildings.

7.2.2 Physic-based channel model

As discussed earlier in Section 2, the conventional multiptah channel model 2 is used to characterize the UWB channels. One reason for this use is that the wireless communications community is so accustomed to Turin's multipath model (14) which is designed for narrowband systems and where no pulse distortion is implicitly assumed for each individual path. To mathematically model the pulse-distortion phenomenon, a generalized version of the channel model (2) is proposed in (2):

$$h(\tau) = \sum_{l=1}^{L} A_l(\tau)\, h_l(\tau) * \delta(\tau - \tau_l) \tag{19}$$

where $h_l(\tau)$ represents an arbitrary function that has finite energy and $*$ symbolizes the convolution. Although, the statistical parameterization of $h_l(\tau)$ is a challenging task, it can be obtained through exact, experimental, numerical or/and asymptotic methods. For instance, $h_l(\tau)$ is obtained in (91) and (92) by asymptotic solutions of MaxwellŠs equations using GTD and Uniform Theory of Diffraction (UTD).

When the bandwidth of the employed transmission waveform goes infinite, the empirical channel models become invalid, since no measurement system has infinite bandwidth. The physics-based model of (19), however, is still valid. For practical applications, it is often sufficient to consider a special form (104)

$$H_l(j\omega) = (j\omega)^{-\alpha_l} \tag{20}$$

$$h_l(\tau) = \frac{1}{\Gamma(\alpha_l)} \tau^{-(1-\alpha_l)} U(\tau) \tag{21}$$

where α_l assumes a positive real value, e.g., $\alpha_l = 1/2$. The $U(\tau)$ is Heaviside's function. The Gamma function is defined as $\Gamma(z) = \int_0^\infty t^{z-1} e^{-t} dt$ where the real part of z is positive, i.e., $\Re(z) > 0$. The function $\tau^{-(1-\alpha_l)} U(\tau)$ has a singularity at $t = 0$, and must be treated as a generalized function. It is also regarded as an unbounded linear operator. In fact, it is the behavior of this operator at $t = 0$ that determines its singular value distribution. Note Eq.(20) is valid for infinite bandwidth or $\omega \to \infty$.
The total channel response for L paths is (104)

$$y(t) = \sum_{l=1}^{L} A_l (I^{\alpha_l} x(t)) * \delta(\tau - \tau_l) \tag{22}$$

where I^{α_l} can be treated as linear fractional integral operators. The fractional integral of the order α is defined as (108)

$$I^\alpha f(x) \equiv \frac{1}{\Gamma(\alpha)} \int_a^x \frac{f(t)}{(x-t)^{1-\alpha}} dt, \quad x > a \tag{23}$$

where $\alpha > 0$ is a real value. This integral is also called Riemann-Liouville fractional integral. The singular value decomposition (SVD) for I^{α_l} has given in (104). Based on its SVD, the capacity of the channel can be thus derived (104). A comprehensive theory is given in (104).

7.2.3 A time-reversal based system paradigm

Often it is more convenient to design a system, based on the channel cross-correlation

$$R_{hh}(t) = h_{forward}(-t; \mathbf{r}_0, \mathbf{r}_1) * h_{reverse}(t; \mathbf{r}_1, \mathbf{r}_0) \tag{24}$$

where $*$ denotes linear convolution, and $\mathbf{r}_0$ and $\mathbf{r}_1$ are the positions of the transceiver. If the channel is reciprocal (99), i.e.,

$$h_{forward}(t; \mathbf{r}_0, \mathbf{r}_1) = h_{reverse}(t; \mathbf{r}_1, \mathbf{r}_0), \tag{25}$$

then, $R_{hh}(t) = h(-t) * h(t)$ reduces to the auto-correlation of the channel impulse response, where the spatial positions are dropped for brevity. The use of auto-correlation simplifies the system design based on the channel impulse response only. One good analogy is the spread-spectrum system that uses the auto-correlation of the spreading codes. The channel impulse response can be viewed as a spatial code.
A so-called generalized RAKE is proposed to compensate for pulse distortion in (81) and (82). This approach however is complex to implement. A time-reversal based system paradigm that exploits the rich multipath and also mitigates pulse distortion is recently used (1), (81), (92)-(96).
The principle of time-reversal is based on the reciprocity of a time division duplexing (TDD) channel. The objective of the proposed research is to achieve (cost-effective and energy-efficient) time-reversal non-coherent reception as an alternative to coherent communications so that the rich multipath of a UWB channel can be fully exploited as a RAKE receiver does. The new system paradigm exploits the hostile, rich-multipath channel (time-reversed CIR) to achieve simplicity. Combining time-reversal with Multiple-Input

Multiple-Output (MIMO) that is the most promising approach to use spectrum and transmission power will further take advantage of spatial-temporal focusing (99)-(104). As a result, time-reversal trades the extremely huge bandwidth of impulse radio and the high power efficiency of MIMO for range extension, while retaining the low-power and low-cost of noncoherent energy-detection (97). This proposed new system paradigm will, through time-reversal, take advantage of the unique impulsive nature of the UWB signals (100; 101), a new dimension of a communication channel. The new frontier of impulsive time-reversal adds more degrees of freedom in exploiting the spatio-temporal dimensions of signals. Finally, the experimental demonstration of time reversal using a UWB system test-bed is carried out over the air recently (103).

7.2.4 Antenna impact

Different from a narrowband system, a UWB system must include antennas as pulse shaping filters. In addition, antennas act as different pulse shaping filters for different angles. Due to unpredictable arriving angles of multi-path, antennas *distort* or *shape* the transmitted pulses differently for different paths, as experimentally observed. Thus, both antennas and propagation environments suggest channel models of (19). The antenna impact on the pulse deformation is studied in (92) and (105). In particular, the antenna as the source of possible distortions on the matching and the radiation pattern is introduced in (105) and also a model for the input impedance and a model to have a representation of the radiation pattern is proposed in (105). The result in (106) show both pulse distortion in the time domain and frequency filtering in the frequency domain. Moreover, a procedure is proposed in (106) how to design a UWB antenna with minimum pulse distortion. The frequency-dependent delay of UWB antennas is investigated in (107). A strong agreement with the delay extracted via time-domain impulse response measurements is shown in (107).

8. Conclusions

In this paper, a comprehensive investigation on the UWB propagation channels measurements is presented. We have reviewed the essential parameters of the channel, like those used in physics-based models, based on a large number of measurement campaigns. These parameters include the important propagation effects in UWB communication channels: 1) Power-loss characteristics including *Path-Loss (PL)*, *large-scale fading* and *small-scale fading*. 2) Temporal characteristics including *multipath arrival rate*, *multipath delay spread (Power Delay Profile (PDP) and Root-Mean-Squared (RMS) delay spread)* and *temporal correlation*. 3) Spatial characteristics including *multipath Angle-of-Arrival (AOA)* and *spatial correlation across the receiver's spatial aperture*. 4) Frequency characteristics including *Frequency-Selectivity (FSE)* and *Pulse-Distortion (PD)*. We have supported this tutorial overview by a integrated summary on measurement results giving insights on UWB fading channel characterization and modeling.

9. Acknowledgment

This work is funded by the Office of Naval Research through a grant (N00014-07-1-0529), National Science Foundation through a grant (ECS-0622125), the Army Research Laboratory and the Army Research Office through a STIR grant (W911NF-06-1-0349) and a DURIP grant (W911NF-05-1-0111), and ONR Summer Faculty Fellowship Program Award. The NSF International Research and Education in Engineering (IREE) program has sponsored the author's visit at Lund University, Sweden during which this paper is finalized.

The second author wants to thank his sponsors Santanu K. Das (ONR), Brian Sadler (ARL), and Robert Ulman (ARO) for helpful discussions. He also wants to thank his hosts T. C. Yang (Naval Research Lab) and Andrew Molisch (Lund) to provide an ideal research environment. The author also wants to thank his former PhD graduate Chenming Zhou for his assistance.

10. References

[1] R. C. Qiu, X. Shen, M. Guizani and T. Le-Ngoc "Introduction," in *UWB Wireless Communications*, Editors: X. Shen, M. Guizani, R.C. Qiu, T. Le-Ngoc, John Wiley, 2006.

[2] R. C. Qiu, H. P. Liu and X. Shen, "Ultra-Wideband for Multiple Access," *IEEE Commun. Mag.*, pp. 2-9, Feb. 2005.

[3] R. C. Qiu, R. Scholtz and X. Shen," Ultra-Wideband Communications-A New Horizon," *IEEE Trans. Vehi. Tech.*, special issue editorial, Vol. 54, No. 5, pp. 1-3, Sept. 2005.

[4] X. Shen, M. Guizani, H. H. Chen, R. C. Qiu, and A. F. Molisch, "Ultrawideband Wireless Communications-Theory and Applications," *IEEE Jour. Selected Areas in Commun.*, special issue editorial, Second Quarter 2006.

[5] J. D. Taylor, *Ultra-Wideband Radar Technology*, Baco Raton, Florida, USA: CRC Press, 2001.

[6] W. Zhuang, X. Shen and Q. Bi, "Ultra-wideband wireless communications," *Wireless Commun. and Mobile Computing*, vol. 3, no. 6, pp. 663-685, 2003.

[7] A. F. Molisch, J. R. Foerster and M. Pendergrass, "Channel Models for Ultra wideband Personal Area Networks," *IEEEWireless Commun. Mag.*, vol. 10, no. 6, pp. 14-21, December 2003.

[8] Z. Irahhauten, H. Nikookar and G. Janssen, "An Overview of Ultra Wide Band Indoor Channel Measurements and Modeling," *IEEE Microwave and Wireless Components Letters*, vol. 14, no. 8, pp. 386-388, August 2004.

[9] A. F. Molisch, "Ultrawideband Propagation Channels-Theory, Measurement, and Modeling," *IEEE Trans. Vehi. Tech.*, vol. 54, no. 5, pp. 1528-1545, Sep. 2005.

[10] A. F. Molisch, D. Cassioli, C.-C. Chong, S. Emami, A. Fort, B.n Kannan, J. Karedal, J. Kunisch, H. G. Schantz, K. Siwiak and M. Z.Win, "A Comprehensive Standardized Model for Ultrawideband Propagation Channels," *IEEE Trans. Ant. Propag.*, vol. 54, no. 11, pp. 3151-3166, Nov. 2006.

[11] A. F. Molisch, "Ultrawideband propagation channels," Submitted to *Proceeding IEEE*, 2008.

[12] H. Hashemi, "The indoor radio propagation channel," *IEEE Proceedings*, vol. 3, no. 7, pp. 943-968, July 1993.

[13] T. S. Rappaport, *Wireless Communications: Principles and Practice*, Upper Saddle River, New Jersey, USA: Prentice Hall PTR, 1996.

[14] G. L. Turin, "Communication Through Noisy, Random-Multipath Channels," *IRE Convention Record*, part 4, pp. 154-166, 1956.

[15] A. A. M. Saleh and R. A. Valenzuela, "A statistical model for indoor multipath propagation," *IEEE Journal on Selected Areas in Commun.*, vol. 5, no. 2, pp. 128U˝ 137, Feb. 1987.

[16] Q. Spencer, B. Jeffs, M. Jensen and A. Swindlehurst, "Modeling the Statistical Time and Angle of Arrival Characteristics of an Indoor Multipath Channel," *IEEE Jour. on Selected Areas in Commun.*, Vol. 18, pp. 347-360, March 2000.

[17] R. J.-M. Cramer, R. A. Scholtz and M. Z. Win, " Evaluation of an Ultra-Wide-Band Propagation Channel ," *IEEE Trans. Ante. and Propag.*, vol. 50 , no. 5 , pp. 561-570, May 2002.

[18] M. Z. Win, R. A. Scholtz and M. A. Barnes, "Ultra-wide Bandwidth Signal Propagation for Indoor Wireless Communications," *IEEE Int. Conf. on Commun.*, pp. 56-60, 1997.

[19] R. J. Cramer, M. Z. Win and R. A. Scholtz, "Impulse radio multipath characteristics and diversity reception," *IEEE Int. Conf. on Commun.*, pp. 21-26, 1998.

[20] R. A. Scholtz, R. J. Cramer and M. Z. Win, "Evaluation of the Propagation Characteristics of Ultra-Wideband Communication Channels," *IEEE Ant. and Propag. Soc. Int. Symp.*, pp. 1650-1654, 1998.

[21] D. Cassioli, M. Z. Win and A. F. Molisch, "A Statistical Model for the UWB Indoor Channel," *IEEE Vehi. Technology Conf.*, pp. 1159-1163, Spring 2001.

[22] D. Cassioli, M. Z. Win and A. F. Molisch, "The Ultra-Wide Bandwidth Indoor Channel: From Statistical Model to Simulations," *IEEE Jour. on Selected Areas in Commun.*, vol. 20, no. 6, pp. 1247-1257, August 2002.

[23] M. Z. Win and R. A. Scholtz, "Characterization of Ultra-Wide Bandwidth Wireless Indoor Channels: a Communication-Theoretic View," *IEEE Jour. on Selected Areas in Commun.*, vol. 20, no. 9, pp. 1613-1627, December 2002.

[24] A. Alvarez, G. Valera, M. Lobeira, R. P. Torres and J. L. Garcia, "Ultra Wideband Channel Model for Indoor Environments," *IEEE Jour. of Commun. and Net.*, vol. 5, no. 4, pp. 1-10, December 2003.

[25] A. Alvarez, G. Valera, M. Lobeira, R. Torres and J. L. Garcia, "New Channel Impulse Response Model for UWB Indoor System Simulations," *IEEE Vehi. Tech. Conf.*, pp. 1-5, Spring 2003.

[26] D. R. J. Estes, T. B. Welch, A. A. Sarkady and H. Whitesel, "Shipboard Radio Frequency Propagation Measurements for Wireless Networks," *IEEE Military Commun. Conf.*, pp. 247-251, 2001.

[27] S. S. Ghassemzadeh, R. Jana, C. W. Rice, W. Turin and V. Tarokh, "A Statistical Path Loss Model for in-home UWB Channels," *IEEE Ultra Wideband Sys. and Tech. Conf.*, pp. 59-64, 2002.

[28] S. S. Ghassemzadeh, L. J. Greenstein, T. Sveinsson and V. Tarokh, " A Multipath Intensity Profile Model for Residential Environments," *IEEE Wireless Commun. and Net. Conf.*, pp. 150-155, 2003.

[29] S. S. Ghassemzadeh and V. Tarokh, "UWB Path Loss Characterization in Residential Environments," *IEEE Int. Microwave Symp. Digest* pp. 365-368, 2003.

[30] S. S. Ghassemzadeh and V. Tarokh, "UWB Path Loss Characterization in Residential Environments," *IEEE Radio Freq. Integ. Circuits Symp.*, pp. 501-504, 2003.

[31] S. S. Ghassemzadeh, L. J. Greenstein, T. Sveinsson and V. Tarokh, "An Impulse Response Model For Residential Wireless Channels," *IEEE Global Telecommun. Conf.*, pp. 1-5, 2003.

[32] S. S. Ghassemzadeh, R. Jana, C. W. Rice, W. Turin, and V. Tarokh, "Measurement and Modeling of an Ultra-Wide Bandwidth Indoor Channel," *IEEE Trans. Commun.*, vol. 52, no. 10, pp. 1786-1796, Oct. 2004.

[33] S. S. Ghassemzadeh, L. J. Greenstein, A. Kavcic, T. Sveinsson and V. Tarokh, " UWB Indoor Path Loss Model for Residential and Commercial Buildings.," *IEEE Vehi. Tech. Conf.*, pp. 3115-3119, Fall 2003.

[34] L. J. Greenstein, S. S. Ghassemzadeh, S.-C. Hong and V. Tarokh, "Comparison Study of UWB Indoor Channel Models," *IEEE Trans. Wireless Commun.*, vol. 6, no. 1, pp. 128-135, Jan. 2007.

[35] V. Hovinen, M. Hamalainen, and T. Patsi, "Ultra Wideband Indoor Radio Channel Models: Preliminary Results," *IEEE Ultra Wideband Sys. and Tech. Conf.*, pp. 75-79, 2002.

[36] C. Prettie, D. Cheung, L. Rusch and M. Ho, "Spatial Correlation of UWB Signals in a Home Environment ," *IEEE Ultra Wideband Sys. and Tech. Conf.*, pp. 65-69, 2002.

[37] J. Keignart and N. Daniele, "Subnanosecond UWB Channel Sounding in Frequency and Temporal Domain," *IEEE Ultra Wideband Sys. and Tech. Conf.*, pp. 25-30, 2002.

[38] J. Kunisch and J. Pamp, "Measurement Results and Modeling Aspects for the UWB Radio Channel," *IEEE Ultra Wideband Sys. and Tech. Conf.*, pp. 19-23, 2002.

[39] H. Luediger, B. Kull, S. Zeisberg and A. Finger, "An Ultra-Wideband Indoor NLOS Radio Channel Amplitude Probability Density Distribution," *IEEE Int. Symp. on Spread Spect. Tech. and Applic.*, pp. 68-72, 2002.

[40] T. B. Welch, R. L. Musselman, B. A. Emessiene, P. D. Gift and D. K. Choudhury, "The Effects of the Human Body on UWB Signal Propagation in an Indoor Environment," *IEEE Jour. Selected Areas in Commun.*, vol. 20, no. 9, pp. 1778-1782, Dec. 2002.

[41] S. M. Yano, "Investigating the Ultra-Wideband Indoor Wireless Channel," *IEEE Vehi. Tech. Conf.*, pp. 1200-1204, Spring 2002.

[42] K. Siwiak, H. Bertoni and S. M. Yano, "Relation Between Multipath and Wave Propagation Attenuation," *IEE Elect. Letters*, vol. 39, no. 1, pp. 142-143, Jan. 2003.

[43] K. Siwiak and D. Mckeown, *Ultra-Wideband Radio Technology*, West Sussex, England: John Wiley and Sons, 2004.

[44] R.-R. Lao, J.-H. Tarng and C. Hsiao, "Transmission coefficients measurement of building materials for UWB systems in 3 -10 GHz," *IEEE Vehi. Tech. Conf.*, pp. 11-14, Spring 2003.

[45] Q. Li and W. S. Wong, "Measurement and Analysis of the Indoor UWB Channel," *IEEE Vehi. Tech. Conf.*, pp. 1-15, Fall 2003.

[46] J. A. Dabin, Ni Nan, A. M. Haimovich, E. Niver, H. Grebel, "The Effects of Antenna Directivity on Path Loss and Multipath Propagation in UWB Indoor Wireless Channels," *IEEE Ultra Wideband Sys. and Tech.*, pp. 305-309, 2003.

[47] J. A. Dabin, A. M. Haimovich and H. Grebel, "A Statistical Ultra-Wideband Indoor Channel Model and the Effects of Antenna Directivity on Path Loss and Multipath Propagation," *IEEE Jour. Selected Areas in Commun.*, vol. 24, no. 4, pp. 752-758, April 2006.

[48] A. H. Muqaibel, A. Safaai-Jazi, A. M. Attiya, A. Bayram and S. M. Riad, "Measurement and Characterization of Indoor Ultra-Wideband Propagation," *IEEE Ultra Wideband Sys. and Tech. Conf.*, pp. 295-299, 2003.

[49] A. Muqaibel, A. Safaai-Jazi, A. Attiya, B. Woerner and S. Riad, "Path-Loss and Time Dispersion Parameters for Indoor UWB Propagation," *IEEE Trans. Wireless Commun.*, vol. 5, no. 3, pp. 550-559, March 2006.

[50] R. M. Buehrer, W. A. Davis, A. Safaai-Jazi and D. Sweeney, "Characterization of the Ultra-wideband Channel," *IEEE Ultra Wideband Sys. and Tech. Conf.*, pp. 26-31, 2003.

[51] B. M. Donlan, D. R. McKinstry and R. M. Buehrer, "The UWB Indoor Channel: Large and Small Scale Modeling," *IEEE Trans. Wireless Commun.*, vol. 5, no. 10, pp. 2863-2873, Oct. 2006.

[52] P. Pagani and P. Pajusco, "Experimental Analysis of the Ultra Wideband Propagation Channel Over the 3.1 GHz - 10 GHz Frequency Band," *IEEE Int. Symp. on Personal, Indoor and Mobile Radio Commun.*, pp. 1-5, 2006.

[53] P. Pajusco and P. Pagani, "Frequency Dependence of the UWB Indoor Propagation Channel," *Second Euopean Conf. Ant. Propag.*, pp. 1-7, 2007.

[54] Y. Suzuki and T. Kobayashi, "Ultra Wideband Signal Propagation in Desktop Environments," *IEEE Ultra Wideband Sys. and Tech. Conf.*, pp. 493-497, 2003.

[55] Z. Irahhauten, J. Dacuna, G. J. M. Janssen and H. Nikookar, "UWB Channel Measurements and Results for Wireless Personal Area Networks Applications," *European Conf. on Wireless Tech.*, pp. 189-192, 2005.

[56] A. Durantini, W. Ciccognani and D. Cassioli, "UWB Propagation Measurements by PN-Sequence Channel Sounding," *IEEE Int. Conf. on Commun.*, pp. 3414-3418, 2004.

[57] D. Cassioli and A. Durantini, "A Time-domain Propagation Model of the UWB Indoor Channel in the FCC-compliant Band 3.6 - 6 GHz based on PN-sequence Channel Measurements," *IEEE Vehic. Tech. Conf.*, pp. 213-217, Spring 2004.

[58] W. Ciccognani, A. Durantini and D. Cassioli, "Time Domain Propagation Measurements of the UWB Indoor Channel Using PN-Sequence in the FCC-Compliant Band 3.6U˝ 6 GHz," *IEEE Trans. Ant. Propag.*, vol. 53, no. 4, pp. 1542-1549, April 2005.

[59] D. Cassioli, A. Durantini and W. Ciccognani, "The role of path loss on the selection of the operating bands of UWB systems," *IEEE Int. Symp. on Personal, Indoor and Mobile Radio Commun.*, pp. 2787-2791, 2004.

[60] A. Durantini and D. Cassioli, "A Multi-Wall Path Loss Model for Indoor UWB Propagation," *IEEE Vehic. Tech. Conf.*, pp. 30-34, Spring 2005.

[61] C.-C. Chong, Y. Kim and S.-S. Lee, "UWB Indoor Propagation Channel Measurements and Data Analysis in Various Types of High-Rise Apartments," *IEEE Vehic. Tech. Conf.*, pp. 150-154, Fall 2004.

[62] A. Bayram, A. M. Attiya, A. Safaai-Jazi and S. M. Riad, "Frequency-Domain Measurement of Indoor UWB Propagation," *IEEE Ant. and Propag. Soc. Symp.*, pp. 1303-1306, 2004.

[63] B. Alavi, N. Alsindi and Kaveh Pahlavan, "UWB Channel Measurements for Accurate Indoor Localization," *IEEE Military Commun. Conf.*, pp. 1-7, 2006.

[64] K. Leechaikitjaroen, S. Promwong, P. Supanakoon, S. Chensirikul and S. Kaewmechai, "Indoor Measurement Results of UWB Impulse Radio for Shot-Range Wireless Systems with RMS Delay Spread and Path Loss," *IEEE Int. Symp. on Commun. and Info. Tech.*, pp. 684-688, 2005.

[65] N. A. Alsindi, D. Birru and D. Wang, "Ultra-Wideband Channel Measurement Characterization for Wireless Magnetic Resonance Imaging Applications," *41th Annual Conf. on Info. Scien. and Sys.*, pp. 135-140, 2007.

[66] S. Bories, A. Sibille and C. Roblin, "UWB Indoor Channel Measurement Study," *IEEE Int. Workshop Ant. tech., Small Ant. and Novel Metamaterials*, pp. 466-469, 2005.

[67] A. Chehri, O. Fortier, H. Aniss and P.-M. Tardif, "UWB Spatial fading and Small Scale Characterization in Underground Mines," *IEEE 23th Biennial Symp. Commun.*, pp. 213-218, 2006.

[68] A. Chehri, O. Fortier and P.-M. Tardif, "Measurement and Modeling of Line-of-Sight UWB Channel in Underground Mines," *IEEE Global Telecommun. Conf.*, pp. 1-5, 2006.

[69] A. Chehri, O. Fortier and P.-M. Tardif, "Large Scale Fading and Time Dispersion Parameters of UWB Channel in Underground Mines," Accepted for publication in *Iint. Jour. Ant. Propag.*, 2008.

[70] H. I. Volos, C. R. Anderson, W. C. Headley, R. M. Buehrer, C. R. C. M. da Silva and A. Nieto, "Preliminary UWB Propagation Measurements in an Underground Limestone Mine," *IEEE Global Telecommun. Conf.*, pp. 3770-3774, 2007.

[71] A. Fort, J. Ryckaert, C. Desset, P. De Doncker, P. Wambacq and L. Van Biesen, "Ultra-Wideband Channel Model for Communication Around the Human Body," *IEEE Jou. Selec. Area Commun.*, vol. 24, no. 4, pp. 927-933, Apr. 2006.

[72] T. Zasowski, F. Althaus, M. Stager, A. Wittneben, G. Troster, "UWB for Noninvasive Wireless Body Area Networks: Channel Measurements and Results," *IEEE Conf. Ultra Wideband Sys. Tech.*, pp. 285-289, 2003.

[73] T. Zasowski, G. Meyer, F. Althaus and A. Wittneben, "UWB Signal Propagation at the Human Head," *IEEE Trans. Microwave Theory Tech.*, vol. 54, no. 4, pp. 1836-1845, Apr. 2006.

[74] Y. P. Zhang and Q. Li, "Performance of UWB Impulse Radio With Planar Monopoles Over On-Human-Body Propagation Channel for Wireless Body Area Networks," *IEEE Trans. Ant. Propag.*, vol. 55, no. 10, pp. 2907-2914, Oct. 2007.

[75] FCC document 00-163, "Revision of part 15 commission rules ET Docket No. 98-153 regarding UWB transmission systems", adopted 5-10-200

[76] M. Lott and I. Forkel, "A Multi-Wall-and-Floor Model for Indoor Radio Propagation," *IEEE Vehi. Tech. Conf.*, pp. 464-468, Spring 2001.

[77] S. Obayashi and J. Zander, "A Body-Shadowing Model for Indoor Radio Communication Environments," *IEEE Trans. Ant. Propag.*, vol. 46, no. 6, pp. 920-927, June 1998.

[78] A. Abdi and M. Kaveh, "Level Crossing Rate in Terms of the Characteristic Function: A New Approach for Calculating the Fading Rate in Diversity Systems," *IEEE Trans. Commun.*, vol. 50, no. 9, pp. 1397-1400, Sep. 2002.

[79] M. Ghavami, L. B. Michael and R. Kohno, *Ultra Wideband Signals and Systems in Communications Engineering*, West Sussex, England: John Wiley and Sons, 2004.

[80] Q. Spencer, M. Rice, B. Jeffs and M. Jensen, "A statistical model for angle of arrival in indoor multipath propagation," *IEEE Vehi. Tech. Conf.*, pp. 1415-1419, Spring 1997.

[81] R. C. Qiu, Q. Zhang and N. Guo, "A Generalized RAKE Receiver for UWB Communications," *IEEE Jour. on Selected Areas in Commun.*, to appear, 2006.

[82] R. C. Qiu, "Pulse Propagation and Detection," *UWB Wireless Communications*, Editors: X. Shen, M. Guizani, R.C. Qiu, T. Le-Ngoc, John Wiley, 2006.

[83] R. C. Qiu, "UWB Wireless Communications," *Design and Analysis of Wireless Networks*, edited by Yi Pan and Yang Xiao, Nova Science Publishers, 2004.

[84] R. C. Qiu, Chapter "UWB Pulse Propagation Processes," *UWB Wireless Communications - A Comprehensive Overview*, Editor: Thomas Kaiser (Germany), Eurasip, 2005.

[85] R. C. Qiu, "A Generalized Time Domain Multipath Channel and Its Application in Ultra Wideband (UWB) Wireless Optimal Receiver Design: Part III System Performance Analysis," *IEEE Trans. Wireless Commun.*, to appear.

[86] R. C. Qiu, "A Generalized Time Domain Multipath Channel and its Application in Ultra Wideband (UWB) Wireless Optimal Receiver Design: Part II Wave- Based System Analysis," *IEEE Trans. Wireless Commun.*, vol. 3, no. 11, pp. 2312-2324, Nov. 2004.

[87] R. C. Qiu, "A Study of the Ultra-Wideband Wireless Propagation Channel and Optimum UWB Receiver Design," *IEEE Jour. on Selected Areas in Commun.s*, vol. 20, no. 9, pp. 1628-1637, December 2002.

[88] R. C. Qiu and I.T. Lu, "Multipath Resolving with Frequency Dependence for Broadband Wireless Channel Modeling," *IEEE Trans. Vehi. Tech.*, vol. 48, no. 1, pp. 273-285, Jan. 1999.

[89] R. C. Qiu and I-Tai Lu, "Wideband Wireless Multipath Channel Modeling with Path Frequency Dependence," *IEEE Int. Conf. on Commun.*, pp. 277 - 281, 1996.

[90] Channel Model Subcommittee, "Status of models for UWB propagation channel," *IEEE 802.15.4a Channel Model (Final Report)*, http://www.ieee802.org/15/pub/TG4a.html, August 2004.

[91] R. C. Qiu, C. Zhou and Q. Liu, "Physics-Based Pulse Distortion for Ultra-Wideband Signals," *IEEE Trans. Vehi. Tech.*, vol. 54, no. 5, September 2005.

[92] R. C. Qiu, "Optimum and Sub-Optimum Detection of Physics-Based Ultra-Wideband SignalsU° A Tutorial Review," *Dynamics of Continuous, Discrete and Impulsive Systems – An International Journal for Theory and Applications (Series B): Special Issue on UWB Wireless Communications*, vol. 12, no. 3, June 2005.

[93] R. C. Qiu, C. M. Zhou, N. Guo, and J. Q. Zhang, "Time Reversal with MISO for Ultra-Wideband Communications: Experimental Results," *IEEE Ant. and Wireless Propag. Letters*, Vol. 5, pp. 269-273, 2006.

[94] N. Guo, R. C. Qiu, and B. M. Sadler, "Reduced-Complexity Time Reversal Enhanced Autocorrelation Receivers Considering Experiment-Based UWB Channels", *IEEE Trans. Wireless Commun.*, vol. 6, no. 12, December 2007.

[95] N. Guo, R. C. Qiu, and B. M. Sadler, "An Ultra-Wideband Autocorrelation Demodulation Scheme with Low-Complexity Time Reversal Enhancement," *IEEE Military Commun. Conf.*, Atlantic City, NJ, Oct. 17-20, 2005.

[96] R. C. Qiu, C. Zhou, N. Guo, and J. Q. Zhang, "Time Reversal with MISO for Ultra-Wideband Communications: Experimental Results," Invited Paper, *IEEE Radio and Wireless Symp.*, San Diego, CA, 2006.

[97] R. C. Qiu, "Time Reversed MIMO for UWB Communications," *2006 Workshop on Short Range UWB Radio Systems*, Santa Monica, CA, April 12, 2006.

[98] C. Zhou and R. C. Qiu, "Spatial Focusing of Time-Reversed UWB Electromagnetic Waves in a Hallway Environment," *IEEE 38th Southeastern Symp. on Sys. Theory*, Cookeville, TN, March 2006.

[99] R. C. Qiu, C. Zhou, J. Q. Zhang, and N. Guo. "Channel Reciprocity and Time-Reversed Propagation for Ultra-Wideband Communications". In *IEEE AP-S International Symposium on Antennas and Propagation, Honolulu, Hawaii*, vol. 1 (June, 2007).

[100] C. Zhou, N. Guo, and R. C. Qiu. "Experimental Results on Multiple-Input Single-Output (MISO) Time Reversal for UWB Systems in an Office Environment". In

IEEE Military Communications Conference (MILCOM07), Orlando, Florida (October, 2007).

[101] C. M. Zhou, B. M. Sadler, and R. C. Qiu. "Performance Study on Time Reversed Impulse MIMO for UWB Communications Based on Realistic Channels". In *IEEE Conf. Military Comm., MILCOM'07*, Orlando, FL (October, 2007).

[102] C. M. Zhou, N. Guo, and R. C. Qiu, "A Study on Time Reversed Impulse UWB with Multiple Antennas Based on Measured Spatial UWB Channels", *IEEE Trans. Vehicular Tech.* (submitted for publication, 2008).

[103] R. C. Qiu and et al. "Time-Reversal Based Range Extension Technique for Ultra-Wideband (UWB) Sensors and Applications in Tactical Communications and Networking". (Quarterly) Technical Report to Office of Naval Research (ONR) Contract No. N00014-07-1-0529,, Tennessee Tech University, Cookeville, TN (April, 2008). 69 pages.

[104] R. C. Qiu, "Physics-Based Channel Models and Fundamental Limits", Book Chapter, "Underwater Acoustic Sensor Networks", Edited by Prof. Yang Xiao, to be published by Auerbach Publications, Taylor & Francis Group, ISBN-10: 1420067117, ISBN-13:978-1420067118, 2008

[105] I. Pele, A. Chousseaud and S. Toutain, "Simultaneous Modeling of Impedance and Radiation Pattern Antenna for UWB Pulse Modulation," *IEEE Ant. and Propag. Soc. Symp.*, pp. 1871-1874, 2004.

[106] W. Lauber and S. Palaninathan, "Ultra-Wideband Antenna Characteristics and Pulse Distortion Measurements," *IEEE Int. Conf. on Ultra-Wideband*, pp. 617-622, 2006.

[107] J. D. McKinney, D. Peroulis and A. M. Weiner, "Time-Domain Measurement of the Frequency-Dependent Delay of Broadband Antennas," *IEEE Trans. Ant. Propag.*, vol. 56, no. 1, pp. 39-47, Jan. 2008.

[108] K. S. Miller and B. Ross, *An Introduction to the Fractional Calculus and Fractional Differential Equations.* (Wiley, NY, 1993).

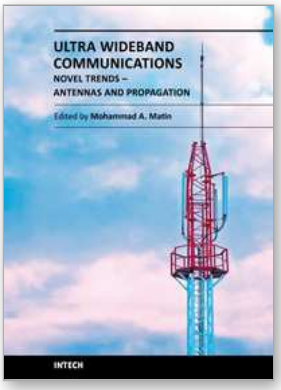

Ultra Wideband Communications: Novel Trends - Antennas and Propagation

Edited by Dr. Mohammad Matin

ISBN 978-953-307-452-8
Hard cover, 384 pages
Publisher InTech
Published online 09, August, 2011
Published in print edition August, 2011

This book explores both the state-of-the-art and the latest achievements in UWB antennas and propagation. It has taken a theoretical and experimental approach to some extent, which is more useful to the reader. The book highlights the unique design issues which put the reader in good pace to be able to understand more advanced research.

How to reference

In order to correctly reference this scholarly work, feel free to copy and paste the following:

Javad Ahmadi-Shokouh and Robert Caiming Qiu (2011). Ultra-Wideband (UWB) Communications Channel – Theory and Measurements, Ultra Wideband Communications: Novel Trends - Antennas and Propagation, Dr. Mohammad Matin (Ed.), ISBN: 978-953-307-452-8, InTech, Available from: http://www.intechopen.com/books/ultra-wideband-communications-novel-trends-antennas-and-propagation/ultra-wideband-uwb-communications-channel-theory-and-measurements

INTECH
open science | open minds

InTech Europe
University Campus STeP Ri
Slavka Krautzeka 83/A
51000 Rijeka, Croatia
Phone: +385 (51) 770 447
Fax: +385 (51) 686 166
www.intechopen.com

InTech China
Unit 405, Office Block, Hotel Equatorial Shanghai
No.65, Yan An Road (West), Shanghai, 200040, China
中国上海市延安西路65号上海国际贵都大饭店办公楼405单元
Phone: +86-21-62489820
Fax: +86-21-62489821